NALoc: Nonlinear Ambient-Light-Sensor-based Localization System

LIN YANG*, Noah's Ark Lab, Huawei Technologies
ZEYU WANG, Hong Kong University of Science and Technology
WEI WANG, Huazhong University of Science and Technology, China
QIAN ZHANG, Hong Kong University of Science and Technology

Visible light position (VLP) is a revolutionary technique which enables many promising applications. As the human eye is sensitive to low-rate changes, VLP systems often convey location information through light flickering over 1 KHz, which induces a heavy burden on the VLP receiver. Existing solutions either rely on the high-resolution cameras or a dedicated photodiode to capture the location information, but the high power consumption and extraction deployment cost hinder their wide adoption. In this paper, we present a light-weight VLP system, *NALoc*, which leverages the ambient light sensor (ALS) readily on many mobile devices to sense high-frequency-modulation location information. To overcome the insufficient sampling ability of ALS, we exploit the nonlinearity of ALS to sense the leaked energy from high frequency($\geq$ 1 KHz) at a low sampling rate(100 Hz). Extensive evaluations demonstrate that our system can achieve a decimeter-level localization accuracy with about 1 mW power consumption, which is 2000 times less than existing camera-based VLP solutions.

CCS Concepts: • **Computer systems organization → Special purpose systems**; • **Hardware → Signal processing systems**; **Sensors and actuators**; **Sensor applications and deployments**; **Sensor devices and platforms**; **Power estimation and optimization**;

Additional Key Words and Phrases: Indoor Localization; Visible Light; Ambient Light Sensor; Nonlinearity; Signal Processing

ACM Reference Format:
Lin Yang, Zeyu Wang, Wei Wang, and Qian Zhang. 2018. NALoc: Nonlinear Ambient-Light-Sensor-based Localization System. *Proc. ACM Interact. Mob. Wearable Ubiquitous Technol.* 2, 4, Article 199 (December 2018), 22 pages. https://doi.org/10.1145/3287077

1 INTRODUCTION

Indoor localization is an innovative technique which enables many promising applications, *e.g.*,navigation, inventory management, and location-based advertising, and greatly impacts peoples' lives [29]. We envision that, in the near future, indoor localization will become an indispensable feature of mobile devices (*e.g.*, mobile phones, smart watches) to further support ubiquitous and continuous localization services, such as real-time trajectory tracking and continuous human/robot navigation. To this end, we need a positioning technology which can simultaneously achieve high accuracy and power efficiency. Also, to eliminate the barrier of wide adaptation by a

*Lin Yang is the corresponding author.

Authors' addresses: Lin Yang, Noah's Ark Lab, Huawei Technologies, Shenzhen, lyangab@connect.ust.hk; Zeyu Wang, Hong Kong University of Science and Technology, Hong Kong, zwangas@connect.ust.hk; Wei Wang, Huazhong University of Science and Technology, China, weiwangw@hust.edu.cn; Qian Zhang, Hong Kong University of Science and Technology, Hong Kong, qianzh@cse.ust.hk.

2474-9567/2018/12-ART199 $15.00
https://doi.org/10.1145/3287077

large number of users, such techniques should not require any hardware modification on commercial-off-the-shelf (COTS) user-end devices, *e.g.*, mobile phone, smart watch, or tablet.

An example use case is the continuous navigation in an office building. Consider a user would like to visit a conference room located in a large office building. He opens his smartphone and starts to navigate. In order to check whether he is on the right path, the user holds the mobile phone on hand while walking and check his current trajectory from time to time.

In such a scenario, the fingerprinting approaches which distinguish each location via profiling the corresponding contextual features, *e.g.*, WiFi signal [5, 32], magnetics [7, 24], barometer [30], or acoustics [22], are limited by the problem of feature instability in the presence of human activities and environmental changes, *e.g.*, power on/off of a personal WiFi AP, or relocation of the furnitures [14]. On the other hand, some model-driven works aim to derive the location of user device through models of received signal strength (RSS) [6], phase [11, 25], or propagation time [15]. While a fine-grained spatial resolution can be achieved, such works often require specialized hardware like antenna arrays and the model can be disturbed by the complex multipath reflections caused by the human movement in office scenario [34].

Through decades of research, visible light positioning (VLP) has shown great potential to fill the gap. The key idea of VLP is to leverage the light fixtures as location landmarks and broadcast a landmark ID through visible light communication. To receive the landmark ID, cameras [12, 18, 33, 36] and specially-designed Photodiode (PD) [13, 34] are often used and various location estimation techniques are proposed. Thanks to the dense deployment of light fixtures in the indoor scenarios and the line-of-sight propagation of visible light, VLP can provide a high localization accuracy and is robust to environmental dynamics. Recent VLP systems demonstrate that a decimeter-level resolution can be achieved [28, 34].

However, a key obstacle for VLP is that, location information is often conveyed through a flickering light, but the human eye is sensitive to low-rate change [28]. Therefore, to prevent interference to the human visual experience, VLP systems often modulate location information through having a light flicker at a high rate (above 1 KHz), which places a high bar on the receiver side. According to the Nyquist-Shannon sampling theorem [21], a signal of frequency f requires a sampling rate of $2f$ at least, *i.e.*, a sampling rate larger than 2 KHz is needed. While existing works have already demonstrated that the sampling ability of a camera can be boosted by leveraging the rolling shutter effect of the CMOS image sensor [12, 18], the power consumption of a camera is significant, normally around 2000 mW [33], which precludes a continuous localization. Moreover, the complex processing of high-resolution images incurs huge computation cost and lengthens the response time. As a remedy, some recent works employ a high-performance photodiode sensor as the receiver [34]. Albeit the sensing power can be reduced to 150 mW, the computation cost of processing a signal sampled at high-frequency is inevitable. Most importantly, these PD sensors are unavailable on COTS devices and the deployment cost may hinder their wide application.

The heavy burden on the receiver side motivates us to quest for a more light-weight VLP solution. In this paper, we present NALoc to enable power-efficient visible light positioning which consumes 2000 times less power than a camera-based approach (or 150 times less power compared to a dedicated-PD-based VLP), without any sacrifice of localization accuracy and reliability. Our key idea lies in the ambient light sensor (ALS), which is already available on many mobile devices [20]. While ALS is only able to sample at low rate (up to 100 Hz), it presents with inherent nonlinear characteristics due to hardware limitations and imperfections. ALS nonlinearity mainly derives from the power amplifier and photodiode inside the ALS chipset and can induce some suspicious higher-order terms of the original frequency. Such a higher-order component further leads to an energy leakage centered at the frequency difference of the original signals, which is termed "*shadow signal*"[1]. Although the original signal flickers at several kilo-hertz, we can ensure the shadow signal always falls within the sampling

[1]The frequency and energy of shadow signal are termed shadow frequency and shadow energy, respectively.

range of ALS by carefully designing the light frequency assignment. By sensing the shadow signal, we find a way to "partially" capture the location information modulated at several Kilo-Hertz at a low sampling rate (100 Hz). Most importantly, the power consumption of ALS ($\leq$ 1 mW) is significantly lower than the camera (2000 mW) or dedicated photodiode (150 mW). In addition, the lower sampling rate of ALS gives less data points to process, which further reduces the computation complexity and response time.

Inspired by this idea, we build NALoc. Several challenges are addressed in our design: (i) The characteristics of ALS nonlinearity is under-discussion and its confounding factors are unexplored. To fill the gap, we dig into the circuit design of ALS and perform both theoretical analysis and experimental validation to investigate the feasibility of using shadow frequency as landmark ID. (ii) Noisy spectrum. Other than the nonlinearity, under-sampling in Analog-to-Digital Converter (ADC), harmonics, ambient noise, and hardware-induced distortions also induce suspicious frequencies into the spectrum. To accurately recognizing the shadow frequency on a noisy spectrum, we exploit the exponential relationship between the shadow energy and ALS gain and introduce a second sampling stage to identify shadow frequency on the spectrum. We further shorten the response time of the second sampling by the careful design of the light landmark distribution. (iii) Landmark capacity. While more landmarks imply we can cover an area with more fine-grained light-cell granularity, the sampling ability of ALS limits the number of available shadow frequencies to be 50 (with 1-Hz interval). Considering the complicated light deployment topology in various indoor scenarios, how to maximize the landmark capacity while ensuring the uniqueness of the landmark is a challenging task. By formulating this problem as an adjacent-distinguishable coloring problem in a graph, we first propose a heuristic landmark assignment algorithm and provide a lower-bound proof, then boost the capacity by 10 times via incorporating the under-sampling result of original frequency into the landmark design.

We prototype NALoc on two COTS ALS sensors which are equipped on the Samsung Galaxy S5, S6, and Apple iPhone 6 Plus. Extensive experiments demonstrate the feasibility and reliability of using shadow frequency as a location landmark under various scenarios. Evaluations in real field tests further show that the median localization error of our system is 20 centimeters, with less than 1-mW sensing power and a positioning time within 1.25 seconds.

Our contributions in this paper can be summarized as follows:

- As far as we know, we are the first to exploit the nonlinearity of ALS to eliminate the heavy burden on the VLP receiver. We have demonstrated that the shadow frequency induced by the ALS nonlinearity can be used as a robust light landmark for VLP purposes.
- To accurately and efficiently recognize a landmark from a noisy spectrum, we propose to leverage the exponential relationship between the shadow energy and ALS gain, and design a 2nd sampling stage with an ALS gain jump to identify the shadow frequency.
- We propose a heuristic light landmark assignment algorithm to maximize the capacity while ensuring the uniqueness of the landmark in a complicated light topology. By incorporating the original frequency, our scheme is able to cover a sufficient number of lights.
- We design and implement NALoc as a light-weight VLP solution based the nonlinear ALS. Evaluation results demonstrate that our system can provides decimeter-level localization with a power consumption 2000 times less than the state-of-the-art camera-based VLP (also 150 times less than the dedicated-PD-based solution).

The rest of paper is organized as follows. We first briefly introduce the operation rationale of ALS and describe its electronic characteristics in Section 2. Then, we explain the core intuition behind our system design and validate its feasibility through experiments in Section 3. The recognition of a landmark and the corresponding landmark assignment algorithm are discussed in Section 4 and 5. Section 6 further details our signal-strength-based localization algorithm in a light cell. In Section 7, we describe our prototype design of NALoc and evaluation

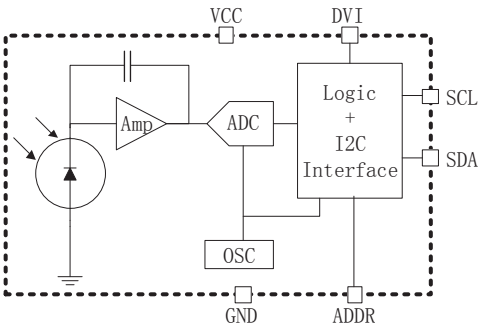

Fig. 1. A typical digital ALS integrates photodiode, amplifier circuitry, ADC, and the interface logic.

setup. Evaluation results are reported in Section 8, followed with a discussion of practical issues in Section 9 and a literature survey in Section 10. At the end, Section 11 concludes this paper.

2 PRELIMINARY

In this section, we start with a brief introduction to the operation rationale of ALS, then we take a close look at two import effects inside the ALS working flow, *i.e.*, nonlinearity of ALS and under-sampling in the Analog-to-Digital converter (ADC).

2.1 Ambient Light Sensor

The Ambient Light Sensor (ALS) is one of the most widely-used sensors in mobile devices with LCD screens, such as mobile phones, smart watches, and tablets. It approximates the human eye response to light under a variety of lighting conditions to provide information about ambient light levels. A common application of ALS is to optimize the operation of the back light of the Liquid Crystal Display (LCD) screen under a variety of environmental lighting situations: the brightness of the screen will be reduced in a dark environment or even turned off when the device is held near the ear, while the back light is tuned on with the presence of a ambient light to maintain good visibility. Since the LCD and its associated back light LEDs are the most power-hungry loads in mobile devices and account for around 40% of the total power consumption, ALS are widely adopted in mobile devices to optimize the battery life [20].

Figure 1 shows a typical circuit design of a digital ALS sensor. It integrates four main modules on a chip: a photodiode, an amplifier, an analog-digital converter (ADC), and the logic/data interface components.

The photodiode is a solid-state device which converts the incident light into an electric current. It consists of a shallow diffused P-N junction. The P-N junction is formed when the P-type dopant with acceptor impurities make contact with the N-type silicon doped with donor impurities. Under the force of inner low electrical potential, the holes and electrons insides the silicon flow across the junction and the resulting charge establishes a depletion region. When a photons of energy greater than 1.1 eV (the band gap of silicon) fall on the depletion area, it is transformed to a pair of electron-hole pairs, which will be swept across the electric field and create the current flow [20]. By measuring this current flow, we can gain an estimation of the incidental light energy.

Before feeding the electric current from photodiode into the ADC, as the current flow generated by the photodiode is too weak, a common practice is to amplify the current by a gain of 2 64 times to ensure that the ADC can measure the signal properly. After that, the analog current flow is sampled into a digital signal by an

ADC and output via the data transmission interface(*e.g.*, I^2C). Although the ADC on modern ALS sensors can support a sampling rate up to 370 Hz [2] [1, 2], the operating system often restricts the sampling rate to 100 Hz [13].

2.2 Nonlinearity of ALS

Ideally, the electrical components inside the ALS work as linear systems satisfying the principle of superposition and are both linear and time invariant. For example, given an input current signal S, the output of an ideal amplifier is:

$$S_{Amp} = A_1 S, \tag{1}$$

where A_1 is a complex gain introduced by the amplifier. Although the amplifier may change the amplitude and phase of the input signal, it does not generate any other new frequencies.

In the real world, however, the electrical component inside the amplifier can only approximate this ideal linear characteristic over a limited range of input amplitudes. Once the input signal exceeds the physical system's limit, the output of the component becomes over-saturated and results in some levels of nonlinearity. Similar nonlinearity happens on the photodiode [8]. In this case, the output signal is expressed as:

$$S_{out} = \sum_{i=1}^{\infty} A_i S^i = A_1 S + A_2 S^2 + \ldots \tag{2}$$

According to our measurement, the third and higher order terms in the output are weak and easily overwhelmed on the noise floor, which leaves us only the first-order and second-order terms (Detailed measurements in Section 3). As the first-order term is linear to the input signal, it is the second-order term which induces spurious energy at new frequencies, *i.e.*, the *shadow signal* we explored in this work(Section 3).

2.3 Under-Sampling and Frequency Aliasing

As we mentioned before, to prevent interference to human visual perception, existing VLP systems often modulate the location information via a light flickering at high frequency (over 1 KHz) [28].According to the Nyquist–Shannon sampling theorem, to fully capture the light flickering at 1 KHz, the sampling rate should be at least 2 KHz. Unfortunately, due to hardware limitations and operating system constraints, the ALS sensors equipped on the COTS mobile devices can only support up to 100-Hz sampling [13], which is obviously far less than the requirement. As a result, the light signal will be sampled at a sub-Nyquist rate and the frequency component is aliased on the spectrum as follows:

$$f_a = \begin{cases} (N+1)f_s - f & f_s/2 < f - Nf_s < f_s \\ f - Nf_s & 0 \le f - Nf_s \le f_s/2 \end{cases} \tag{3}$$

where f_a is the aliased frequency corresponding to the original frequency f and f_s is the sampling rate and N is nonnegative integers. Such frequency aliasing induces ambiguity in the light frequency and makes it insufficient to sever as a location identifier. For example, under a sampling rate of 100 Hz, a light frequency of 1047 Hz will fold back to 47 Hz, while another light of 1053 Hz is also aliased to 47 Hz.

3 CORE INTUITION & FEASIBILITY

To eliminate the heavy burden of the VLP receiver, NALoc mainly leverages nonlinearity of ALS to sense the high-frequency-modulated location information at a low sampling rate. In this section, we explain the core intuition behind this idea in detail and validate its feasibility through theoretical analysis and experimental measurements.

[2]This frequency is limited by the fact that the minimal integration time of ALS is 2.7 ms.

3.1 Shadow Frequency as Landmark

For simplicity, let us first consider a scenario in which two lights flicker at f_1 and f_2 Hz, each of which is above 1 KHz. When these two lights arrive simultaneously at the ALS sensor, the ALS input becomes:

$$S = S_1 + S_2 = \sin(\omega_1 t) + \sin(\omega_2 t), \tag{4}$$

where $\omega_1 = 2\pi f_1$ and $\omega_2 = 2\pi f_2$.

The nonlinearity further renders ALS output consists of a set of spurious power series. The higher-order components of the power series are quite minor related to the noise, only the first-order and the second-order terms dominate the output signal, that is:

$$\begin{aligned} S_{out} &= \sum_{i=1}^{\infty} A_i S^i = A_1 S + A_2 S^2 + \dots \\ &\approx S + S^2 \\ &= (S_1 + S_2) + (S_1 + S_2)^2 \\ &= [\sin(\omega_1 t) + \sin(\omega_2 t)] + [\sin(\omega_1 t) + \sin(\omega_2 t)]^2 \\ &= [\sin(\omega_1 t) + \sin(\omega_2 t)] + [\sin^2(\omega_1 t) + \sin^2(\omega_2 t) + 2\sin(\omega_1 t)\sin(\omega_1 t)] \end{aligned} \tag{5}$$

While the first-order term only generates frequencies at f_1 and f_2, expanding the second-order term leaves us with two squared terms doubles the original frequencies and a cross-term. By applying the product-to-sum identities, we can see that the cross-term generates frequencies at both $f_1 + f_2$ and $f_1 - f_2$. Expanding above equation leads to :

$$S_{out} = \underbrace{\left[\sin(\omega_1 t) + \sin(\omega_2 t)\right] + \left[1 - \frac{1}{2}\cos(2\omega_1 t) - \frac{1}{2}\cos(2\omega_2 t) + \cos\left((\omega_1 + \omega_2)t\right)\right.}_{\text{High-frequency components beyond the ALS' sampling ability}} \underbrace{- \left.\cos\left((\omega_1 - \omega_2)t\right)\right]}_{\text{Shadow signal}}, \tag{6}$$

where $\omega_1 = 2\pi f_1$ and $\omega_2 = 2\pi f_2$.

Given the original flickering frequencies (f_1 and f_2) are over 1 KHz, these high-frequency components, *i.e.*, f_1, f_2, $2f_1$, $2f_2$, and $f_1 + f_2$, are far beyond the sampling range of ALS, but the shadow signal at $f_{shadow} = f_1 - f_2$ is possible to be sensed by ALS if the difference between f_1 and f_2 is less than the half of ALS sampling rate: $|f_1 - f_2| \leq f_s/2$.

In light of this observation, we carefully assign the light frequencies in a way such that the flickering frequency of each light is above 1 KHz, but the frequency difference between adjacent lights is within the sensing ability of ALS. By exploiting the shadow frequency as a landmark ID, our system is able to sense the location information at a very low sampling rate. Moreover, as the shadow signal is caused by the ALS nonlinearity, it only exists inside the ALS sensor. The human eye does not exhibit such nonlinear characteristics and can not perceive low-frequency shadow signals, thus a good visual experience can be retained.

Note that, although we can observe the original flickering frequency on the ALS spectrum, the frequency aliasing caused by under-sampling renders it insufficient to serve as a landmark ID. For example, all the original flickering frequencies at 1010 Hz, 1090 Hz, ... ,$(N * 100 + 10)$ Hz, $\big((N + 1) * 100 - 10\big)$ Hz, are perceived as 10 Hz by an ALS sampling at 100 Hz. It is hard to identify the original frequency from the ALS side.

Apparently, to serve as a landmark, the shadow frequencies of different locations need to be unique, which implies the frequency difference between each pair of adjacent lights should be distinguishable inside the whole area. To this end, we design a light frequency assignment scheme to automatically assign flickering frequencies to each adjacent light fixture (Section 5). In real applications, NALoc first recognizes the shadow frequencies from

a noisy spectrum (Section 4), then compares the combination of shadow frequencies with a predefined landmark-location database to get the light-cell-level location information. After that, a geometric received-signal-based localization model (cf. Section 6) can further help our system to derive fine-grained location coordinates with respect to the landmark.

3.2 Feasibility Validation

Before realizing our system, we first need to validate several assumptions:

1) *Can the shadow signal be observed on COTS device?* As the shadow signal is derived from the second-order term caused by ALS nonlinearity, its power needs to be significant enough to ensure the shadow signal can be clearly observed.
2) *Can the shadow signal be observed under the distance and illuminance level in a typical indoor scenario?* Considering a typical indoor VLP application of a 3-meter ceiling height, the sensing distance should be up to 2.5 meters and the indoor illuminance varies from 100 to 800 Lux [26]. We wonder whether this idea still works under such an application scenario?
3) *Is the nonlinearity prevalent on different ALS sensors, especially the ones adopted on the COTS devices?* To work with the COTS mobile devices, it is necessary to validate the nonlinear characteristics are consistent on various ALS sensors equipped on today's mobile devices.

3.2.1 Existence of Shadow Signal on COTS Device. To examine the significance of shadow signal, we drive two 6-Watt LED lights with an FPGA board, setting their flickering frequencies to be 1016 Hz and 1053 Hz, respectively. An AMS TMG3992 ALS sensor from a Samsung Galaxy S6 is used as a receiver and placed 2.0 meters away from the lights. Figures 2(a) and 2(b) show the power spectrum distribution of the ALS reading when only one light is flickering. We can see that, as the ALS samples at 100 Hz, the flickering frequency of light 1 (1016 Hz) is folded back to $1016 - 100 * 10 = 16$ Hz, while the frequency of light 2, $f_2 = 1053$ Hz, is aliased to $100 * 11 - 1053 = 47$ Hz. Similar frequency aliasing also occurs on the harmonic frequencies. When two lights flicker simultaneously (Figure 2(c)), we can observe the aliased frequencies at both 16 Hz and 47 Hz, as well as an obvious signal at 37 Hz, which is the shadow signal caused by the nonlinearity. We note that the frequency of the shadow signal is equal to the difference between the original flickering frequencies, *i.e.*, $1053 - 1016 = 37$ Hz, which corresponds to our previous analysis in Section 3.1. More importantly, the power of the shadow signal is significantly higher than the noise floor, which confirms a good signal-to-noise ratio of shadow signal.

3.2.2 Confounding Factors of Shadow Signal. According to the rationale of ALS nonlinearity, the shadow signal is determined by the strength of the input signal, which is significantly affected by the illuminance level, sensing distance, and ALS gain. To understand how these factors affect the shadow signal, we compute the signal-to-noise Ratio (SNR) of the shadow signal by placing the ALS sensor to various distances and setting its gain to different gain level. The measurement results are reported in Figure 3.

Several insights can be made from this figure: i) The illuminance level drops exponentially as the distance increases, which satisfies the power law of the light propagation model. ii) With the growth of distance, the SNR of both the original light frequency and shadow frequency decrease significantly. iii) For the SNR under 111x gain, we observe a first increasing then decreasing trend. This is because at a close distance, a high ALS gain leads to a serious value overflow which reduces the SNR. As the distance increase, the overflow phenomenon is alleviated and the SNR is improved. iii) By setting proper ALS gain, we can always ensure that the SNR of the shadow signal is larger than 3dB, even under a distance of 2.5 meters. These observations indicate that the shadow signal can be obviously sensed under a typical indoor localization scenario.

3.2.3 Consistency on Different Devices. Another important question to ask is whether such nonlinearity presents on various ALS sensors equipped on today's mobile devices. To this end, we choose two representative ALS

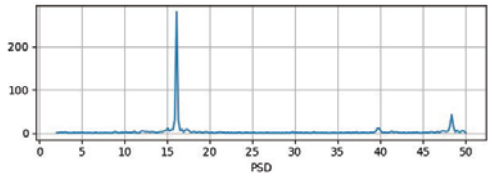

(a) The spectrum of ALS readings when only light 1 flickers at 1016 Hz.

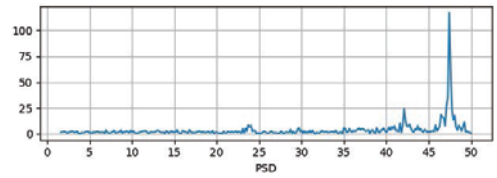

(b) The spectrum of ALS readings when only light 2 flickers at 1053 Hz.

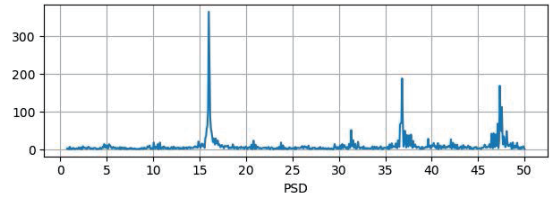

(c) The spectrum of ALS readings when both lights flicker simultaneously.

Fig. 2. The spectrum of ALS readings. We can clearly observe a shadow signal at 37 Hz.

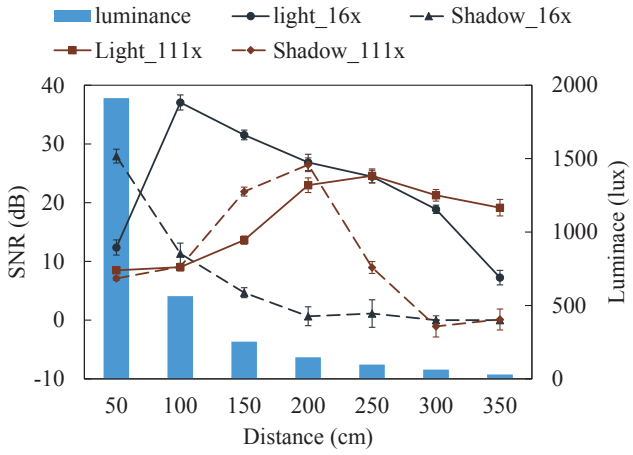

Fig. 3. The SNR of shadow signal under different distances, illuminance levels, and gain settings.

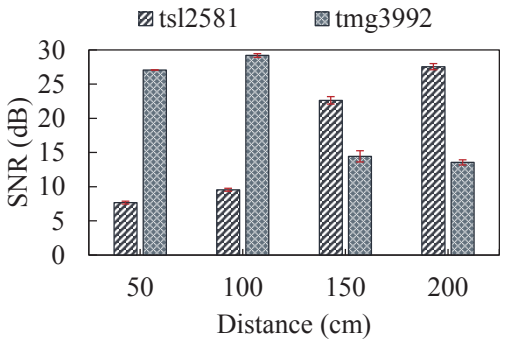

Fig. 4. The SNR of shadow signal on two representative ALS sensors under various distance.

sensors from the most popular mobile phone manufacturers: the AMS TMG3992 from Samsung Galaxy S5/S6/Note 4 [2] and the AMS TSL2581 light sensor on the Apple iPhone 6 Plus [1].

Figure 4 shows the SNR of shadow signal on these two sensors. We can clearly see that the shadow signal can be observed on both sensors and their SNR values are larger than 3dB under various distances. Previous researches also suggest that, as the nonlinearity derives from the hardware imperfection, it is prevalent on various sensors, especially for the power amplifier [8, 19]. All of these observations imply a great potential for the wide deployment of our system on various devices.

4 DISCRIMINATING LIGHT LANDMARKS

To derive the location information, the NALoc receiver needs to identify the landmark, *i.e.*, frequency of shadow signal from the ALS data. However, this is not trivial work because other than the nonlinearity, the frequency aliasing caused by under-sampling, harmonics of original light frequencies, ambient noise, as well as the hardware-induced distortions, also induce suspicious frequencies in the ALS, leading to a noisy spectrum. In this section, we explain how to leverage the ALS gain jump to recognize the shadow frequency from a noisy spectrum and then propose an optimized frequency selection algorithm to further accelerate the

4.1 Recognizing the Shadow Frequency with the 2^{nd} Sampling

One possible way is to identify the shadow frequency through the energy level. While in theory the energy level of the shadow signal is smaller than the original light frequency, the frequency aliasing may introduce ambiguity to this approach because each round of frequency fold-back caused by under-sampling introduces some energy loss. Also, this approach is not robust under high-noise scenarios.

As an alternative, we propose to recognize the shadow frequency by exploring the exponential relationship between the shadow energy and ALS gain. Consider two light signals $S_1 = A_1 \cos \omega_1 t$ and $S_2 = A_2 \cos \omega_2 t$, where A_1 and A_2 are the signal strength of S_1 and S_2. Let α_1 and α_2 represent the amplification effect of ALS gain on the S_1 and S_2, respectively. Substituting them into the Equation(5) gives:

$$S_{out} = (\alpha_1 A_1 \cos \omega_1 t + \alpha_2 A_2 \cos \omega_2 t) \tag{7}$$

$$+ (\alpha_1 A_1 \cos \omega_1 t)^2 + (\alpha_2 A_2 \cos \omega_2 t)^2 \tag{8}$$

$$+ 2\alpha_1 \alpha_2 A_1 A_2 \cos \omega_1 t \cdot \cos \omega_2 t \tag{9}$$

On the one hand, from the first-order term (Equation(7)), we know that the amplitude of original light frequencies are:

$$\begin{cases} Amp(f_1) = \alpha_1 A_1, \\ Amp(f_2) = \alpha_2 A_2 \end{cases} \tag{10}$$

On the other hand, we can expand the cross term (Equation(9)) with trigonometric identities and derives the amplitude of the shadow frequency as follows:

$$\begin{aligned} CROSS\_TERM &= 2\alpha_1 \alpha_2 A_1 A_2 \cos \omega_1 t \cdot \cos \omega_2 t \\ &= \alpha_1 \alpha_2 A_1 A_2 [\cos(\omega_1 - \omega_2)t + \cos(\omega_1 + \omega_2)t] \\ \Rightarrow \quad & Amp(f_1 - f_2) = \alpha_1 \alpha_2 A_1 A_2 \end{aligned} \tag{11}$$

The amplitude of shadow frequency is determined by the product of ALS gain effects on both light signals. If we reduce the ALS gain by $1/n$, then the amplification effects of S_1 and S_2 become $\frac{\alpha_1}{n}$ and $\frac{\alpha_2}{n}$, which leads to corresponding amplitude changes:

$$\begin{cases} Amp\prime(f_1) = \alpha_1 A_1 / n, \\ Amp\prime(f_2) = \alpha_2 A_2 / n, \\ Amp\prime(f_1 - f_2) = \alpha_1 \alpha_2 A_1 A_2 / n^2 \end{cases} \tag{12}$$

Obviously, we can see an exponential relationship between the shadow energy and the ALS gain. Note that, while the amplitude of frequency $(f_1 + f_2)$ also presents similar exponential relationship to the ALS gain, it far exceeds the sampling ability of ALS and thus its amplitude becomes very small after many folds of frequency aliasing. Besides, further expanding of the second-order terms also suggests that the other high-frequency components, *e.g.*, $2f_1$, $2f_2$, do not present such exponential changes.

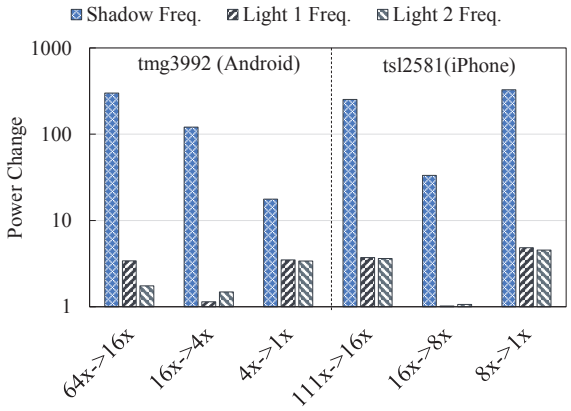

Fig. 5. The feasibility of 2^{nd} sampling. We can clearly observe that the amplitude of shadow signal drops more significantly than the light signals during the ALS gain jump.

This observation enlightens us to perform another round of sampling with ALS gain jump. In particular, we first samples the ALS with a certain gain value for 1 second (*i.e.*, 1^{st} sampling), then we reduce the gain value by half and perform a 2^{nd} sampling. By comparing the FFT results of these two samplings, we can identify the frequency of shadow signal.

To validate this idea, we employ two COTS ALS sensors and set their gain to different values during the 1^{st} and 2^{nd} sampling. Figure 5 compares the amplitude changes in the shadow signal and light signals. Note the y-axis is in log scale. We find that the amplitude of shadow signal changes exponentially with respect to the gain drop, while the light frequencies vary relatively linearly. This result confirms the feasibility of recognizing the shadow frequency by 2^{nd} sampling.

4.2 Accelerating the 2^{nd} Sampling

While the previous experiment demonstrates the 2^{nd} sampling works, an important question is *how long does it take?* One intuitive answer might be 1 second because it gives a 1-Hz resolution on the spectrum[3]. However, the 1^{st} sampling already takes 1 second (because we need 1-Hz resolution in this stage), the duration of the 2^{nd} sampling should be as short as possible.

To this end, we notice that, after the 1^{st} sampling, we already know the exact index of each frequency on the spectrum. For the 2^{nd}, we only need to know which frequency drops most significantly. Therefore, the resolution of 2^{nd} sampling is determined by the interval between shadow signal and light signals on the spectrum. A larger interval implies a more coarse FFT resolution and thus a shorter time for the 2^{nd} sampling.

Apart from this, we also observe that the same shadow frequency can be derived from various combinations of light frequencies. For example, both combinations of (1001Hz, 1008Hz) and (1040Hz, 1047Hz) can generate a shadow signal of 7 Hz, but the interval between shadow and light frequency of (1001Hz, 1008Hz) is 1 Hz while the interval of the second combination is 33 Hz.

[3]the resolution of FFT is determined by f_s/n, where the f_s is the sampling rate and n is the number of samples.

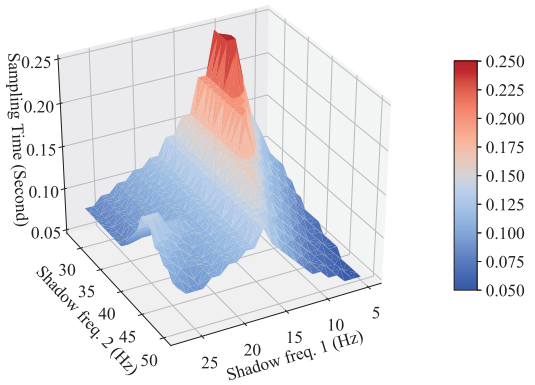

Fig. 6. The duration of 2^{nd} sampling in a 3-lights setting. We can clearly observe that the amplitude of shadow signal drops more significantly than the light signals during the ALS gain jump.

In light of these observations, we search for a optimal light frequency combination which maximizes the shadow-light interval for each shadow frequency. This can be formulated as:

$$\begin{aligned} max. \quad & min(|aliased(f_1) - \Delta f|, |aliased(f_2) - \Delta f|) \\ s.t. \quad & \Delta f = |f_1 - f_2| \end{aligned} \tag{13}$$

where Δf is the shadow frequency. Since the number of available shadow frequencies is limited, this optimization problem can easily be solved in a brute-force way.

Figure 6 shows the time distribution of the $2^n d$ sampling for a 3-light setting. The average duration of the 2^{nd} sampling is 0.1174 seconds, while the min duration only lasts for 0.05 seconds and max duration is 0.25 seconds.

5 ASSIGNING LIGHT FREQUENCIES

After solving the optimization problem in Equation. 13, we have a list of shadow frequencies and corresponding light frequencies. Due to the limitation of ALS sampling rate and FFT resolution we use (1 Hz), only 50 shadow frequencies are available. Now the question is how to use these shadow frequencies as landmarks.

To serve as a location landmark, two requirements should be met: i) each landmark should be unique in the whole area, and 2) the capacity of landmark should be sufficient to cover all the lights inside a building. According to previous measurement, a typical indoor VLP system should be able to cover 500 lights [33].

To find the solution, given any floor plan and light deployment topology, we can transform it into a graph problem as follows: We first represent each light as a node. For each pair of adjacent lights in the floor plan, if they can be perceived simultaneously by an ALS sensor with a similar illuminance level , we then create an edge between these two lights. Besides, let a color set $C = \{c_1, c_2, ..., c_{50}\}$ denotes the available shadow frequencies, this further becomes a coloring problem.

Definition 5.1. *Coloring Problem:* Given a graph $G(V, E)$ and a color set $C = \{c_1, c_2, ..., c_{50}\}$, find a coloring scheme that can cover as many vertices as possible while ensuring the color combination of each pair of adjacent edges is unique in the graph. We define the *capacity* as the number of vertices that can be covered.

Based on this formulation, several observations can be made:

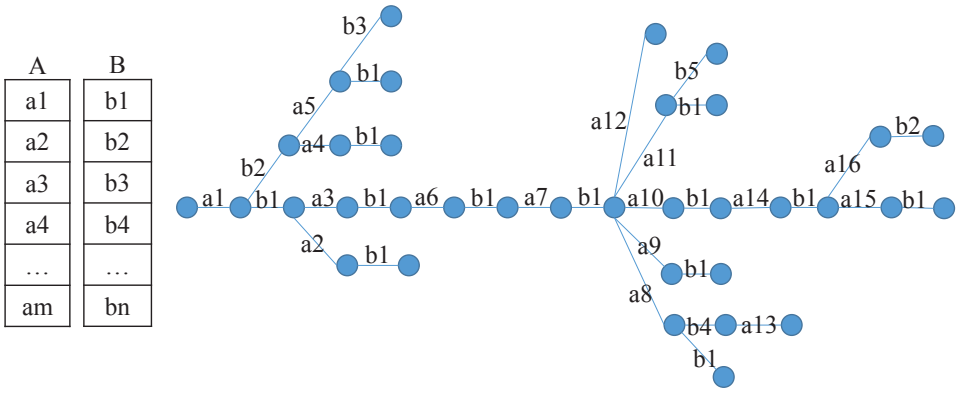

Fig. 7. An example of landmark assignment. The coloring of each pair of adjacent edges is unique in the MST tree.

- Given a real floor plan and light deployment topology, we can formulate it as a connected graph because normally there will be a path between any two lights in a building.
- The capacity highly depends on the degrees of the vertices in the graph. A vertex with a higher degree has more adjacent edges, suggesting more color combinations are needed. In general, a higher degree implies a smaller capacity.
- Uniquely coloring a connected graph is equivalent to uniquely coloring the spanning tree of this graph. This is because that, under our scenario, assigning coloring to edges is *de facto* determining the frequency difference between lights (nodes). For example, considering a triangular cycle formed by node A, B, and C. If the frequency difference between AB and BC are defined to be Δf_1 and Δf_2, then the frequency difference on edge AC is also determined, *i.e.*, $\Delta f_1 + \Delta f_2$.

Considering the complicated graph structure, it very hard to give a general closed-form solution for the capacity. Therefore, we turn to propose a heuristic algorithm and analyze its capacity.

The key idea is to employ a pair of shadow frequencies as a landmark, which implies that our system requires at least three lights to identify a location. Also, instead of coloring the connected graph, we choose to color its spanning tree. As a high vertex degree can limit the capacity, we aim to coloring a spanning tree with minimal vertex degree.

To this end, we define a weight $w(e)$ for each edge e in the graph as:

$$w(e) = \sqrt{\delta_l^2 + \delta_r^2} \tag{14}$$

where δ_l and δ_r denote the degree of the left-hand and right-hand side nodes of edge e, respectively. Then, we employ the Prim's algorithm [17] to find a spanning tree with the minimal vertex degree (MST).

On top of this MST tree, we assign light frequencies in a breadth-first way. For each node level, we first select a specific coloring set from A and B. If set A is chosen, then we iteratively select unused frequencies from set A and assign them to edges within this level. If the selected set is B, then only the edges within the same branch need unique colors. Once a color is assigned, we mark the color combination of the current edge and its $parent(e_{ij})$ used. Algorithm 1 further describe this process in detail and Figure 7 shows an example of the landmark assignment.

ALGORITHM 1: Landmark Assignment Algorithm.

Input: Available landmark set L, Light deployment graph G, Primary landmark set A, Secondary landmark set B ;
Output: Landmark assignment T'

$A \leftarrow L,\ B \leftarrow reverse(L),$;
$T' \leftarrow \emptyset$;
Define a weight $w(e)$ for each edge e as Equation. 14;
Find the minimal spanning tree (MST) T for the given graph G;
Current set $S \leftarrow A$, current landmark $l = 0$;
Declare all the edges are unlabeled;
while *Some edges in T are not labeled yet* **do**
    `// Travel all the edges in a Breadth-first way`
    for *i-th level in the MST tree T:* **do**
        if $S == A$ **then**
            Pick the next available landmark in S: $l = next(S)$;
        end
        for *each j-th edge* e_{ij} *in the i-th level:* **do**
            Assign l to the edge e_{ij}: $T'.add(e_{ij}, l)$;
            Declare e_{ij} is labeled;
            Mark the color combination of the current edge and its $parent(e_{ij})$ used;
        end
        Switch to another landmark Set: $(S == A)?S = B : S = A$;
    end
end
Result: T'

Apparently, the capacity of this algorithm is d:etermined by the vertex degree in the MST tree and can be estimated as:

$$Cap = \frac{\binom{50}{2}}{\sum_{v \in \{V\prime | \delta(v) > 2\}} \binom{\delta_v}{2} / |V\prime|} \tag{15}$$

where δ_v denotes the degree of vertex v and $V\prime$ is the set of vertices whose degree is larger than 2.

According to our measurements, the degree of vertices are often less than 5, the average degree is around 3. In this case, the capacity of our algorithm is 516, which is sufficient for our purpose. However, in an extreme case of the kind that the lights are deployed in a star topology, forming a star graph in which the max vertex degree larger than 50, our system can only support up to 50 lights. This gives the lower bound of our algorithm: minimal capacity is 50.

To further boost the capacity of our algorithm, we propose to incorporate the aliased light frequency into the landmark. In particular, a landmark includes the shadow frequencies between lights, as well as the frequency aliasing result of the original light frequencies. By dividing the spectrum into 10 bins and checking which bin the aliased frequency falls into, we can further boost the capacity by 10 times, *i.e.*, minimal capacity = $50 * 10 = 500$, which is sufficient for our purposes.

6 3D LOCALIZATION

By identifying the landmark and comparing it with a predefined landmark-location database, we can derive the corresponding light cell. After that, NALoc uses simple trilateration models to derive a fine-grained 3D location inside the light cell. The key idea is to leverage the received energy of each light source. The location of each

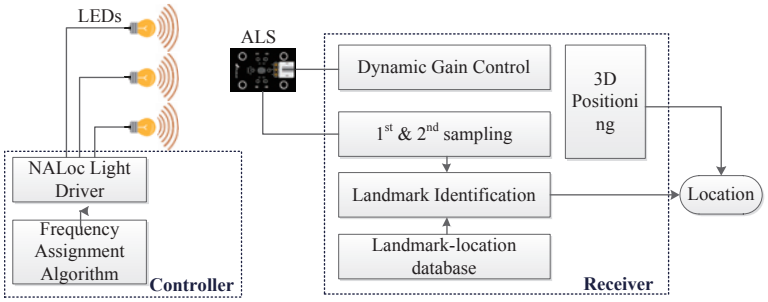

Fig. 8. The system architecture of NALoc, which consists of the NALoc controller and receiver.

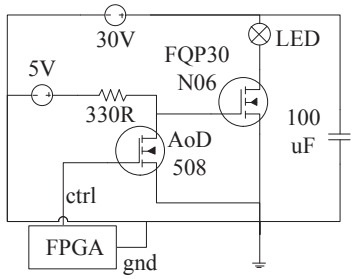

Fig. 9. The circuit design of NALoc light driver for a light.

LED bulb is the global 3-D coordinates related to the flickering frequency. The received energy is the magnitude of its aliased frequency on the FFT results which is related to the distance and orientation between the ALS and the LED bulb. Its model is similar to the optical model of existing VLP systems [13]. As a result, the Received Signal Strength (RSS) measured of one LED bulb is

$$P_r = Asin(c\pi)\frac{p(\theta)q(\phi)}{d^2}; \tag{16}$$

where P_r is the received power which is estimated by the magnitude from FFT, A is the constant related to its maximum emission power, f is the LED bulb frequency, c is the duty cycle, $p(\theta)$ is the incidence angle response function of the ALS, $q(\phi)$ is the irradiation angle response function of the LED bulb and d is the distance between the LED bulb and the receiver.

Based on the model, our localization algorithm is designed as a Levenberg-Marquardt optimization process[16]. We do not provide the details of the localization algorithm since it is not our contribution. As a whole, the localization algorithm needs at least 3 LED bulbs to solve the problem.

7 IMPLEMENTATION & DEPLOYMENT

Figure 8 shows the design of our prototype. It consists of two main components: 1) a **NALoc controller**, which controls the flickering of each light fixture according to the light frequency assignment. 2) a **NALoc receiver**, which recognizes the landmark from the ALS reading and derives fine-grained location information according to the 3D localization algorithm.

The **NALoc controller** implements two function components: a) the frequency assignment algorithm, which determines the flickering frequencies of light fixtures according to the MST tree, and b) the NALoc light driver, which is designed to be an integrated circuit on which we implement the controlling algorithm for the light flickers. Its circuit design is showed in Figure 9. The core part is an Altera Cyclone II FPGA board (EP2C8T144C6), on which we implement the controlling algorithm in Verilog and control a 6w LED light with two MOSFET n-channel gates. There are 5 lights in total for our current prototype implementation.

The **NALoc receiver** includes 5 function units: a) as the ALS gain can affect the significance of nonlinearity, a *dynamic gain control* is used to optimize the ALS gain according to the light intensity[4]. The receiver replies on the *1st & 2nd sampling* to perform a 2-stage sampling on the ALS readings and identify the landmark through *Landmark identification*. By matching the landmark in the *landmark-location database*, the corresponding light

[4]This gain can be easily set by a heuristic rules, so this part is omitted in this paper.

cell can be recognized. With the help of the *3D positioning algorithm*, we can further derive a fine-grained location information.

Note that to realize our system in real world, it needs some retrofitting works to connect the existing light fixtures to a NALoc driver. According to our current implementation, the circuit can be built at a low cost (≤ 1 US dollar) and the FPGA ($150) can further be replaced by other low-cost micro-controllers, *e.g.*, ARM STM32. Such a driver can support up to hundreds of lights, depending on the number of output pins on the control board. We believe such a retrofitting cost is relatively low and affordable, compared to the receiver-side cost.

Yet another issue for the deployment is the density requirement for the light landmarks. The number of light frequencies can be captured by our system depends on not only the FoV angle, but also the lights' height/density. Their relationship can be described by the follow equation:

$$d = \pi\left(h\tan(\frac{\pi v}{360})\right)^2 \tag{17}$$

where d is the area in which at least 2 light frequencies should be captured, h is the ceiling height, and v is the working FoV angle of our system.

Given the working FoV of our system is 60°, a typical indoor scenario of ceiling height of 2.5 meters gives a deployment density of 6.545 m^2 and a ceiling height of 3 meters further enlarges this area to 9.425 m^2.

While this requirement can be generally met for most areas in an indoor scenario, *e.g.*, an academic building on campus, we do notice that there still exist some areas that are only covered by a single light, *e.g.*, some corners, a small kitchen, or the end of aisle. Such areas can be easily identified in advance via an on-site measurement.

To address this issue, one intuitive way is to set the frequencies of these single-light areas to be distinctive. While this can decrease the overall capacity of our system, it can be a feasible choice if the capacity is sufficient. Another alternative is to combine the built-in motion sensors and explore the continuous trajectory to derive current location if only one light frequency detected. The error accumulation from the dead reckoning can be eliminated by recalibrating with previously recognized landmarks.

8 PERFORMANCE EVALUATION

In this section, we first investigate the feasibility of sensing the shadow signal under various conditions, then move to the evaluation of landmark identification accuracy. After that, we perform a field test to evaluate NALoc's localization precision, followed by a power consumption analysis.

8.1 Sensing of Shadow Signal under Various Conditions

Although we have demonstrated the shadow frequency can be sensed over different ALS sensors over various distances, we wonder whether some other sensing conditions, *i.e.*, light incident angle, ALS gain setting, and user mobility, can affect its significance. To this end, we employ the same experiment setup as Section 3.2.2 to examine these issues.

8.1.1 Field-of-View Angle. As the photodiode inside ALS owns a limited field-of-view angle (FoV), it has been evidenced that the response of ALS drops obviously as the light incident angle moves out of the ALS' FoV. To examine the working FoV angle, we place a ALS sensor 2 meters away from the light, and rotate it to different angles with respect to the light-incident direction. Figure 10 shows the corresponding SNR of light/shadow signals under different angles. We find that the shadow signal can maintain a good SNR value ($\geq$ 3dB) when the incident angle varies from 60° to 120°, suggesting a FoV of 60°. As soon as the light incident angle move out of this range, the shadow signal attenuated significantly.

Note that many smartphone cameras only support an FoV around 70° [33]. For example, the FoV of Lumia 1020 is 64° and the Apple iPhone 6 owns an FoV of 63.54° [3, 12]. A smaller FoV of 56° is also employed in a recent dedicated-photodiode-based work [34]. Like many existing works, this issue can be easily addressed by

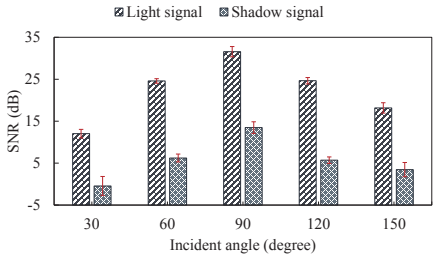

Fig. 10. The SNR of shadow/light signal under different incident angle.

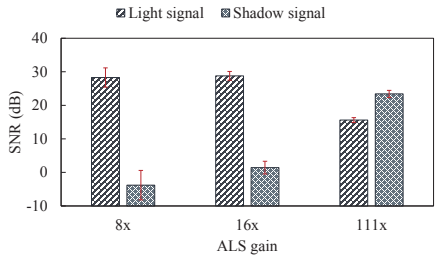

Fig. 11. The SNR of shadow/light signal under user movement.

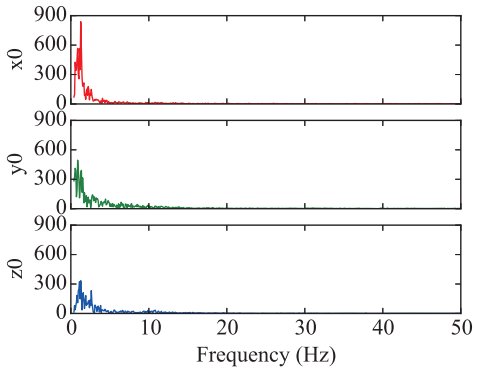

Fig. 12. The spectral energy of user mobility concentrates below 5Hz.

facing the smartphone screen towards the light lamp [5]. While such a requirement can slightly decrease user experience, this should not be a killing issue as the localization can be done within 1.25 seconds.

8.1.2 ALS Gain. Another confounding factor is the gain setting of ALS. It not only controls the amplification ratio of the power amplifier, but also determines the sensitivity of the photodiode inside the ALS [1], both of which can significantly affect ALS nonlinearity. To explore the effect of this parameter on the significance of shadow signals, we place an AMS TSL2581 ALS sensor (from iPhone 6 Plus) 2-meters away from the light and set its gain to different values. There are 4 tunable gain values in this sensor: 1x, 8x, 16x, and 111x. As the gain of 1x does not changes the input signal at all, it is often used under extreme high illuminance scenario, *e.g.*, outdoor with direct sunlight may give an illuminance over 2000 Lux. As the normal indoor illuminance level is less than 1000 Lux [26], we do not include 1x into our experiment. Figure 13 shows the increasing trend of the shadow signal with respect to the growth of ALS gain. This meets our expectation as a higher amplification gain and sensitivity can easily make the ALS reading out of its linear scope, causing serious nonlinearity. Meanwhile, we also notice the light SNR starts to decrease as the ALS gain is larger than 16x. This is because when the ALS gain is 111x, the ALS reading overflows and the highest energy, *i.e.*, the energy of the light frequency, is cut off.

8.1.3 User Mobility. In the real application, the users will hold the NALoc receiver, *i.e.*, their mobile devices, in hand to localize. Thus, the inference from user mobility is inevitable. To understand how it affects our system, we first quantify how much inference can be caused by the user mobility. To this end, we ask several volunteers to

[5] the ALS sensor is often installed near the screen

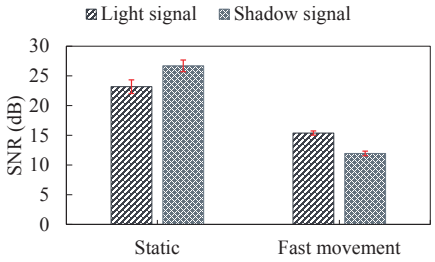

Fig. 13. The SNR of shadow/light signal with user mobility.

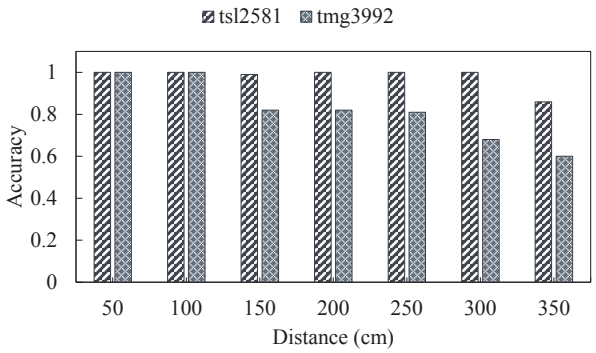

Fig. 14. The identification accuracy of landmark over distance.

walk in normal speed while texting messages on his/her phone and shows an example power spectrum of the corresponding accelerometer readings in Figure 12. We observe that the most energy of the human movement concentrates at the frequencies lower than 5 Hz. This fact is also confirmed by many other works [27, 35].

One intuitive way is to incorporate a high-pass filter to eliminate the interference of user mobility. We understand this might slightly hurt our capacity as we need to give up any frequency less than 5 Hz, but the capacity lost is small and still acceptable. To evaluate the effectiveness of this approach, we implement a high-pass filter with a cutting frequency of 5 Hz in our prototype and intentionally moves the ALS randomly and quickly during the ALS sensing. Figure 11 compares the SNR of light/shadow signal under static and movement scenarios. While we can clearly observe a quality drop in the movement scenario, the SNR of signal quality is still larger than 3 dB, suggesting it is easy to distinguish.

8.2 Accuracy of Landmark Identification

To provide an accurate localization service, one vital step is to identify the landmark correctly. In this section, we evaluate the identification accuracy of the landmark under various scenarios.

8.2.1 Working Distance. Considering a typical indoor scenario of a 3-meter high ceiling, a working distance of landmark identification should be at 2 meters. To examine how NALoc performs under different distances. We place the ALS sensor at different distance and set the corresponding ALS gain heuristically. Figure 14 shows that our system can maintain a good identification accuracy over 83% even under a sensing distance of 2.5 meters, which satisfies our application requirement.

8.2.2 Light Incident Angle . According to the previous experiment in Section 8.1.1, ALS can detect the shadow signal within an FoV of 60°. We wonder if we can correctly identify the landmark within the ALS FoV. To this end, we place the ALS sensor at different angles with respect to the light direction. Figure 15 shows that the landmark identification accuracy is above 95% from 60° to 120° and drops significantly outside this range, which perfectly corresponds to our previous measurements in Section 8.1.1.

8.2.3 Interference. In this experiment, we simulate multiple interferences common in the real application, *e.g.*, light change due to the user movement, ambient noise from sunlight, or even artifacts caused by coexisting compact fluorescent lamps (CFLs). Figure 16 shows the accuracy of landmark identification under such interference and we observe that our system is robust. This is because, i) by incorporating the high-pass filter, we can easily eliminate the interference of user mobility. ii) While the sunlight is unmodulated and does not induce any

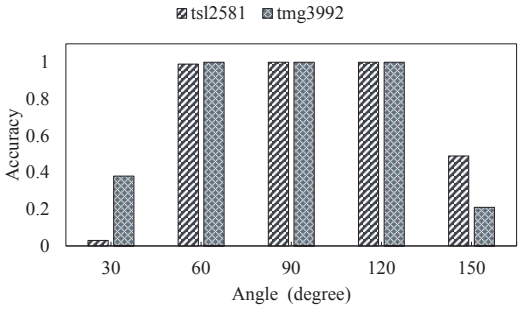

Fig. 15. The landmark identification accuracy under different field-of-view angles.

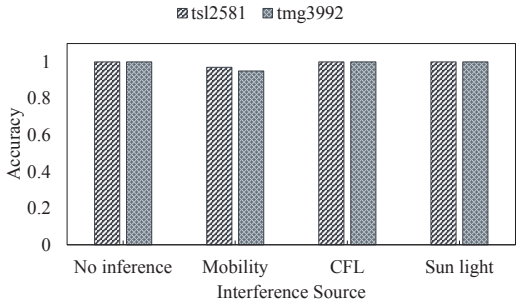

Fig. 16. The landmark identification accuracy with user mobility/ambient lights.

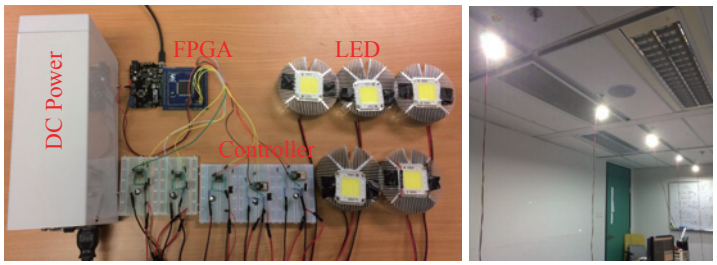

Fig. 17. Prototype of NALoc.

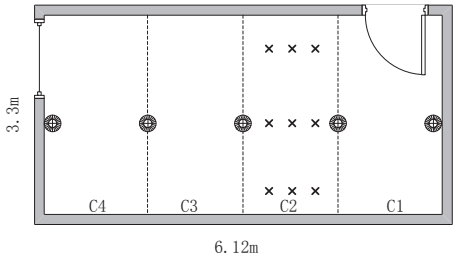

Fig. 18. Experiment setup of NALoc.

frequency on the spectrum, the CFL flickers at a fixed frequency of 50 or 60 Hz, which can also be eliminated by a notch filter [21].

8.2.4 Real-Field Test. To comprehensively evaluate the performance of our system, we setup a prototype system as shown in Figure 17. In a conference room of 3.3 meter × 6.12 meter, we deploy 5 LED light on the ceiling, which divide the whole room into 4 cells, each of which is further partitioned into 9 grids (see Figure 18 Under this setting, we measure the SNR of the shadow signal in each grid and compute the localization accuracy. Since the main focus of our system is to identify the landmark ID from the shadow signal, we only define the localization accuracy of our system as the probability of correctly recognizing a corresponding landmark ID on the grid.

Figure 19 show the corresponding accuracy in each grid. We can see that, in different cells, our system can maintain a good performance, the overall mean accuracy is 98%, which is sufficient for localization. However, we also notice that, in some grids , *e.g.*, the identification of C1L2 is only 73%. This is because this location is directly under one of the LED light with no adjacent light on its right-hand side, which means the light energy from this light dominates the power spectrum and hinders the identification of shadow signal.

8.3 Localization

To further evaluate the localization precision of our system, we derive a 3D location based on the prototype and experiment setup in Section 8.2.4. Figure 20 shows the CDF of localization errors in centimeters. We can see that 50% of the error is within 20 cm, while 90% of the localization is within a 35-cm area.

A milestone VLP system [12], which utilizes a mobile camera to decode the on-off-keying location information embedded in the light, can provide a fine-grained spatial resolution with a median error of 7 cm when the user

C4			C3			C2			C1		
1.00	1.00	1.00	1.00	0.86	1.00	1.00	1.00	1.00	1.00	1.00	1.00
1.00	1.00	1.00	0.94	1.00	1.00	1.00	1.00	1.00	1.00	1.00	0.73
1.00	1.00	1.00	1.00	0.83	0.88	1.00	1.00	1.00	1.00	1.00	1.00

Fig. 19. The landmark identification accuracy 1in different locations.

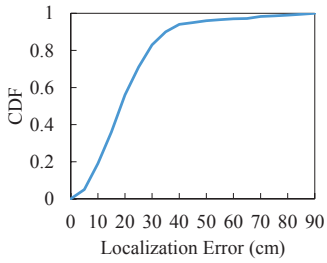

Fig. 20. The CDF of localization errors.

Table 1. The localization accuracy of some recent VLP systems.

Name	Receiver	50% of error (cm)	90% of error(cm)
Luxapose [12]	camera	30	75
Pixel [28]	camera	8	30
LiTell [33]	camera	15	26
Pulsar [34]	dedicated PD	26	65
NALoc	ALS	20	35

is under the light. However, once the user moves out, the median error increases to about 30 cm. The Pixel is another recent VLP work which explores the polarization of light to discriminate the light landmarks. Their experiments shows that the 50% of localization error are less than 8 cm, and 90% of them are within 30 cm. Table 1 compares our system with recent VLP works.

We understand our system does not provide the highest localization accuracy compared to the camera-based works. However, we are not questing for the best localization accuracy. Instead, we try to find a balance between localization accuracy and power efficiency.

8.4 Power Consumption

Figure 21 compares the sensing power of ALS with the camera and dedicated photodiode [34]. We can see that, compared to the power-hungry camera which consumes more than 2000 mW and dedicated photodiode of 150mW, the ALS sensor only needs less than 1mW, which is significantly less that the others by many orders.

To further understand the power consumption inside the ALS, we measure the power consumption of each component by setting the ALS to different states. As we can see from Figure 22, the major power is spent on powering the ALS sensor while the sensing and communication only consumes 10% of the total power. This implies there is still room for more power optimization, *e.g.*, we can turn the ALS off during the idle time and only power it up during the positioning.

9 DISCUSSION

As a first step to leveraging the ALS nonlinearity for indoor localization, while our evaluation results demonstrate the promise of NALoc, it still has several issues which are worthy to further investigate:

- **Resistance to Environment Dynamics**. As the light fixtures are often densely deployed in the indoor scenarios and the visible light propagates along a directed-line path, VLP is able to provide a more stable signal quality [13, 33, 34]. Also, the fact that most light fixtures are installed on the ceiling further alleviates

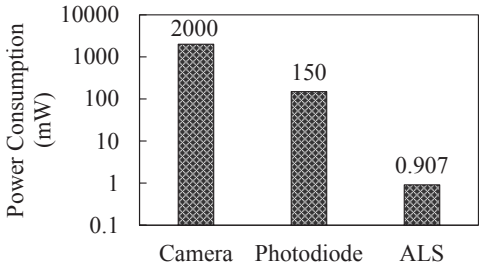

Fig. 21. Sensing power consumption of different sensors.

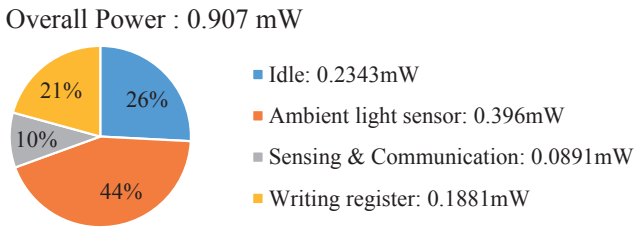

Fig. 22. The power consumption of each process insides the ALS sensor.

the signal quality issue caused by user blockage. As a result, the main interference source of VLP derives from the ambient: we are nowadays surrounded by many artificial lights, such as: advertisement screen and televisions. These artificial ambient lights can generate suspicious frequencies on the spectrum. Such suspicious frequencies may be quite similar to the light frequency, in terms of both amplitude and frequency,which can confuse the identification of a landmark. One possible solution is to employ the RGB light sensor which is already integrated with some ALS chipset [2] to further distinguish frequency on each color channel. Since the light inference from such artificial lights often contains light energy of more than one color, it is possible that we can identify the interference with RGB light sensors. Solving this problem can improve the robustness of our system, and we will solve this problem in the future.

- **Working with Different Kinds of Lights**. For now, our system only works with LED lights. Although the adaption of LED is a leading trend in the illuminance market, there are still plenty of traditional lamps being used in the world. By making our system compatible with these lights, NALoc can be deployed at lower cost in many scenarios. We leave this for further exploration.
- The **Field-of-View (FoV) Angle** is determined by the directional response of the photodiode inside ALS sensor. As the incident angle of light exceeds a working FoV of Photodiode, its signal strength decreases exponentially and significantly lower the SNR of shadow signal, which hinders the discrimination of the shadow frequency. Our experiment in Section 8.1.1 indicates the working FoV of our system is 60°. To further boost the FoV angle, several ways can be explored: (i) the most direct way is to use the other ALS sensors with wider FoV. For example, the AMS TSL2581 [1] used on the Apple iPhone 6 Plus owns a wider directional response spanning from -90° to 90°, and can work under a large FoV angle. (ii)We also notice that, to suppose extra application, *e.g.*, gesture recognition, many existing COTS ALS sensors integrate multiple photodiodes on the same chipset [2], which enables a possibility to combine the multiple signals from different photodiodes to alleviate the noise interference and increase the SNR of the shadow signal, which can extend the working FoV range.
- **Usability**. As our system intrinsically relies on the visible light, it presents some limitations when compared with the wireless-based localization systems. Due to the transmission and penetration characteristics of the RF signal, the wireless-based approaches can localize the user's position without a line-of-sight propagation between the landmark and the receiver, which enables many promising applications in both passive and active localization scenarios. On the contrary, visible-light-based positioning requires the user to face the mobile device to the light source and can only be used for the active positioning. However, such a line-of-sight propagation also empowers NALoc with a good signal quality [34] and a high resilience to environment dynamics. Also, as many light fixtures are installed on the ceiling, the signal blockage problem can be alleviated. In addition, while the wireless-based approaches need a power-hungry wireless module,

e.g., WiFi/Cellular/Bluetooth [5, 32], to sense the location information modulated in the RF signal, our solution employs a built-in ALS sensors as receiver, which consumes < 1 mW during working and can help extend the battery life.

10 RELATED WORK

Indoor localization has been studied for many years[29] and existing works can be divided into two categories, fingerprinting and modeling. Fingerprinting approaches extract features from multiple sources such as acoustics[22] or RF-signal[4, 5] to represent each location landmark. However, such features are unstable in reality, due to the noise from the environment, and are often not discriminative enough to offer fine location granularity[14]. In addition, they need to gather the fingerprinting from all locations which involves a huge overhead. Modeling approaches estimate the distance between the receiver and the landmarks based on the propagation model of the received signal strength[9], phase[11, 25] or time[15]. To achieve high location precision, such models often require specialized hardware like antenna arrays. On the other hand, the received data from such approaches suffer from the multi-path effect due to the environment[14].

Our work is more related to visible light positioning. Recent studies[12, 13, 18] show that visible-light-based localization is a promising approach with higher accuracy since visible light is more directional and stable. The difference between the existing works and NALoc is the system requirements of the end user. Most of the works[12, 28, 31, 33] utilize the camera as the receiver and achieve sub-meter level accuracy based on the rolling shutter effect. However, the power consumption is high for camera viewing and capturing. Some works[10, 13, 23] exploit the traditional light sensor as the receiver or make a particular modification. Compared with these approaches, NALOC just uses the general ambient light sensor from commercial smartphones or wearables to achieve localization. As a result, the requirements of mobile devices is largely improved.

11 CONCLUSION

In this paper, we have explored the possibility of nonlinear characteristics of ambient light sensors to enable a highly accurate and power-efficient VLP system. The key idea lies in using the shadow frequency induced by the ALS nonlinearity as the location landmark. Our feasibility experiments demonstrate that the shadow frequency can be sensed correctly and robustly under various scenarios. Field test further shows that our system can provide a comparable decimeter-level accuracy, while only consuming less than 1mW sensing power. Also, the low sampling rate of ALS relieves the processing load during positioning, leading to a fast response time(1.25 seconds). While there is still plenty of room for improvement, we believe NALoc presents great promise towards robust and light-weight indoor localization with visible light.

REFERENCES

[1] AMS. 2010. AMS TSL2581 Ambient Light Sensor. http://ams.com/eng/Products/Light-Sensors/Ambient-Light-Sensors/TSL2581. (2010).
[2] AMS. 2014. AMS TMG3992 Optical Sensor. http://ams.com/eng/Products/Light-Sensors/Gesture-Color-Sensors-Proximity-Detection/TMG39921. (2014).
[3] AnandTech. 2013. Understanding Camera Optics & Smartphone Camera Trends. http://ams.com/eng/Products/Light-Sensors/Gesture-Color-Sensors-Proximity-Detection/TMG39921. (2013).
[4] Paramvir Bahl and Venkata N Padmanabhan. 2000. RADAR: An in-building RF-based user location and tracking system. In *INFOCOM 2000. Nineteenth Annual Joint Conference of the IEEE Computer and Communications Societies. Proceedings. IEEE*, Vol. 2. Ieee, 775–784.
[5] Yin Chen, Dimitrios Lymberopoulos, Jie Liu, and Bodhi Priyantha. 2012. Fm-based indoor localization. In *Proceedings of the 10th international conference on Mobile systems, applications, and services*. ACM, 169–182.
[6] Krishna Chintalapudi, Anand Padmanabha Iyer, and Venkata N Padmanabhan. 2010. Indoor localization without the pain. In *Proceedings of the sixteenth annual international conference on Mobile computing and networking*. ACM, 173–184.
[7] Jaewoo Chung, Matt Donahoe, Chris Schmandt, Ig-Jae Kim, Pedram Razavai, and Micaela Wiseman. 2011. Indoor location sensing using geo-magnetism. In *Proceedings of the 9th international conference on Mobile systems, applications, and services*. ACM, 141–154.
[8] Robert R Hayes and David L Persechini. 1993. Nonlinearity of pin photodetectors. *IEEE photonics technology letters* 5, 1 (1993), 70–72.

[9] Kiran Raj Joshi, Steven Siying Hong, and Sachin Katti. 2013. PinPoint: Localizing Interfering Radios.. In *NSDI*. 241–253.
[10] Soo-Yong Jung, Swook Hann, and Chang-Soo Park. 2011. TDOA-based optical wireless indoor localization using LED ceiling lamps. *IEEE Transactions on Consumer Electronics* 57, 4 (2011).
[11] Manikanta Kotaru, Kiran Joshi, Dinesh Bharadia, and Sachin Katti. 2015. Spotfi: Decimeter level localization using wifi. In *ACM SIGCOMM Computer Communication Review*, Vol. 45. ACM, 269–282.
[12] Ye-Sheng Kuo, Pat Pannuto, Ko-Jen Hsiao, and Prabal Dutta. 2014. Luxapose: Indoor positioning with mobile phones and visible light. In *Proceedings of the 20th annual international conference on Mobile computing and networking*. ACM, 447–458.
[13] Liqun Li, Pan Hu, Chunyi Peng, Guobin Shen, and Feng Zhao. 2014. Epsilon: a visible light based positioning system. In *NSDI'14 Proceedings of the 11th USENIX Conference on Networked Systems Design and Implementation*. 331–343.
[14] Hongbo Liu, Yu Gan, Jie Yang, Simon Sidhom, Yan Wang, Yingying Chen, and Fan Ye. 2012. Push the limit of WiFi based localization for smartphones. In *Proceedings of the 18th annual international conference on Mobile computing and networking*. ACM, 305–316.
[15] Andreas Marcaletti, Maurizio Rea, Domenico Giustiniano, Vincent Lenders, and Aymen Fakhreddine. 2014. Filtering noisy 802.11 time-of-flight ranging measurements. In *Proceedings of the 10th ACM International on Conference on emerging Networking Experiments and Technologies*. ACM, 13–20.
[16] Jorge J Moré. 1978. The Levenberg-Marquardt algorithm: implementation and theory. In *Numerical analysis*. Springer, 105–116.
[17] Christos H Papadimitriou and Kenneth Steiglitz. 1982. *Combinatorial optimization: algorithms and complexity*. Courier Corporation.
[18] Niranjini Rajagopal, Patrick Lazik, and Anthony G. Rowe. 2014. Visual light landmarks for mobile devices. In *Proceedings of the 13th international symposium on Information processing in sensor networks*, Vol. 2014. 249–260.
[19] Nirupam Roy, Haitham Hassanieh, and Romit Roy Choudhury. 2017. Backdoor: Making microphones hear inaudible sounds. In *Proceedings of the 15th Annual International Conference on Mobile Systems, Applications, and Services*. ACM, 2–14.
[20] Rohm Semiconductor. 2013. Ambient Light Sensor (ALS) Applications in Portable Electronics. (2013).
[21] Steven W Smith et al. 1997. The scientist and engineer's guide to digital signal processing. (1997).
[22] Stephen P Tarzia, Peter A Dinda, Robert P Dick, and Gokhan Memik. 2011. Indoor localization without infrastructure using the acoustic background spectrum. In *Proceedings of the 9th international conference on Mobile systems, applications, and services*. ACM, 155–168.
[23] Bo Xie, Guang Tan, and Tian He. 2015. Spinlight: A high accuracy and robust light positioning system for indoor applications. In *Proceedings of the 13th ACM Conference on Embedded Networked Sensor Systems*. ACM, 211–223.
[24] Hongwei Xie, Tao Gu, Xianping Tao, Haibo Ye, and Jian Lu. 2016. A reliability-augmented particle filter for magnetic fingerprinting based indoor localization on smartphone. *IEEE Transactions on Mobile Computing* 15, 8 (2016), 1877–1892.
[25] Jie Xiong and Kyle Jamieson. 2013. Arraytrack: a fine-grained indoor location system. Usenix.
[26] Lin Yang, Wei Wang, Zeyu Wang, and Qian Zhang. 2018. Rainbow: Preventing Mobile-Camera-based Piracy in the Physical World. In *Computer Communications, IEEE INFOCOM 2018-The 37th Annual IEEE International Conference on*. IEEE.
[27] Lin Yang, Wei Wang, and Qian Zhang. 2016. VibID: user identification through bio-vibrometry. In *Information Processing in Sensor Networks (IPSN), 2016 15th ACM/IEEE International Conference on*. IEEE, 1–12.
[28] Zhice Yang, Zeyu Wang, Jiansong Zhang, Chenyu Huang, and Qian Zhang. 2015. Wearables Can Afford: Light-weight Indoor Positioning with Visible Light. In *Proceedings of the 13th Annual International Conference on Mobile Systems, Applications, and Services*. 317–330.
[29] Ali Yassin, Youssef Nasser, Mariette Awad, Ahmed Al-Dubai, Ran Liu, Chau Yuen, Ronald Raulefs, and Elias Aboutanios. 2017. Recent Advances in Indoor Localization: A Survey on Theoretical Approaches and Applications. *IEEE Communications Surveys and Tutorials* 19, 2 (2017), 1327–1346.
[30] H. Ye, T. Gu, X. Tao, and J. Lu. 2014. B-Loc: Scalable Floor Localization Using Barometer on Smartphone. In *2014 IEEE 11th International Conference on Mobile Ad Hoc and Sensor Systems*. 127–135. https://doi.org/10.1109/MASS.2014.49
[31] Masaki Yoshino, Shinichiro Haruyama, and Masao Nakagawa. 2008. High-accuracy positioning system using visible LED lights and image sensor. In *Radio and Wireless Symposium, 2008 IEEE*. IEEE, 439–442.
[32] Moustafa Youssef and Ashok Agrawala. 2005. The Horus WLAN location determination system. In *Proceedings of the 3rd international conference on Mobile systems, applications, and services*. ACM, 205–218.
[33] Chi Zhang and Xinyu Zhang. 2016. LiTell: robust indoor localization using unmodified light fixtures. In *Proceedings of the 22nd Annual International Conference on Mobile Computing and Networking*. 230–242.
[34] Chi Zhang and Xinyu Zhang. 2017. Pulsar: Towards Ubiquitous Visible Light Localization. In *Proceedings of the 23rd Annual International Conference on Mobile Computing and Networking*. ACM, 208–221.
[35] Li Zhang and *et al.* 2015. AccelWord: Energy Efficient Hotword Detection through Accelerometer. In *Proceedings of the 13th Annual International Conference on Mobile Systems, Applications, and Services*. ACM, 301–315.
[36] Shilin Zhu and Xinyu Zhang. 2017. Enabling High-Precision Visible Light Localization in Today's Buildings. In *Proceedings of the 15th Annual International Conference on Mobile Systems, Applications, and Services*. ACM, 96–108.

Received February 2018; revised August 2018; accepted October 2018